PAPER

Check for updates

Revolutionizing sample preparation: a novel autonomous microfluidic platform for serial dilution†

Dries Vloemans, [iD] Alexander Pieters,
Francesco Dal Dosso and Jeroen Lammertyn [iD]*

Dilution is a standard fluid operation widely employed in the sample preparation process of many bio(chemical) assays. It serves multiple essential functions such as sample mixing with certain reagents at specific dilution ratios, reducing sample matrix effects, bringing target analytes within the linear assay detection range, among many others. Traditionally, sample processing is performed in laboratory settings through manual or automated pipetting. When working in resource-limited settings, however, neither trained personnel nor proper laboratory equipment are available limiting the accessibility to high-quality diagnostic tests. In this work, we present a novel standalone and fully automated microfluidic platform for the stepwise preparation of serial dilutions without the need for any active elements. Stepwise dilution is achieved using the coordinated burst action of hydrophobic burst valves to first isolate a precisely metered volume from an applied sample drop and subsequently merge it with a prefilled diluent liquid. Downstream, expansion chambers are used to mix both reagents into a homogeneous solution. The dilution module was characterized to generate accurate and reproducible (CV < 7%) dilutions for targeted dilution factors of 2, 5 and 10×, respectively. Three dilution modules were coupled in series to generate three-fold logarithmic ($\log_5$ or $\log_{10}$) dilutions, with excellent linearity ($R^2 > 0.99$). Its compatibility with whole blood was furthermore illustrated, proving its applicability for automating and downscaling bioassays with complex biological matrices. Finally, autonomous on-chip serial dilution was demonstrated by incorporating the self-powered (i)SIMPLE technology as a passive driving source for liquid manipulation. We believe that the simplicity and modularity of the presented autonomous dilution platform are of interest to many point-of-care applications in which sample dilution and reagent mixing are of importance.

Introduction

In many chemical and biological assays, dilution is a common fluid operation during sample pre-processing, which involves repetitive manual or automated pipetting steps. Preparing a range of concentration standards, performing

KU Leuven, Department of Biosystems, Biosensors Group, Willem de Croylaan 42, box 2428, 3001 Leuven, Belgium. E-mail: jeroen.lammertyn@kuleuven.be

† Electronic supplementary information (ESI) available: Word document (.docx) with additional information on colorimetric characterization experiments on the dilution accuracy and non-specific binding behaviour of fluorescein in the microfluidic circuit. Video S1 illustrates the general working principle of the dilution module. Video S2 illustrates the fluorescence microscopy videos used for the assessment of the mixing efficiency in the mixing unit. Videos S3 and S4 show the reagent compatibility experiments with low surface tension liquids and whole blood samples. Video S5 shows the dilution process with whole blood sample. Video S6 illustrates the automated serial dilution process in the fully-integrated microfluidic chip driven by the SIMPLE pump. See DOI: https://doi.org/10.1039/d4lc00195h

sample dilutions to extend the dynamic range of immunological assays and reducing matrix effects when working with crude samples (*i.e.*, whole blood) all require multiple consecutive iterations of reagent metering and mixing.[1] When having access to proper laboratory equipment (*e.g.*, micropipettes) and trained personnel this is a straightforward and routine procedure. However, in contamination-prone resource-limited point-of-care (POC) settings (*e.g.*, at home), where neither the knowledge nor equipment is available, an automated standalone platform for sample dilution would be of huge interest.[1,2]

To realize this, the use of microfluidics has been of enormous interest because of its capability to downscale and automate complex liquid handling. Three main microfluidic approaches have been explored to automate and integrate the dilution process within miniaturized microfluidic chips. First, controlled diffusive mixing between two or more parallel laminar flows is used to generate concentration gradients along the length of a microchannel.[3,4] This

approach is typically exploited to study the effects of chemical and drug concentrations on cell behaviour and toxicity.[5–7] By repeated splitting and recombination of these flows within a branched microfluidic channel network, a variety of linear, parabolic or even periodical concentration profiles can be generated.[4,8] Kim *et al.* proposed an alternative design based on the same diffusion principle to realize stepwise linear and logarithmic serial dilutions.[9–11] Although diffusion-based diluters can generate complex concentration profiles, their continuous flow operation requires a constant supply of multiple reagents with external pumping equipment, which is not ideal for operation in resource-limited settings.

To avoid continuous reagent consumption, microfluidic dilution systems with integrated valves were developed to first meter and subsequently mix discrete reagent volumes in a stepwise manner. Paegel *et al.* used the peristaltic action of five pneumatic valves to mix a metered sample volume (400 nL) with a diluent through a microfluidic ring-shaped structure.[12] By using a ladder-shaped microfluidic design, this system enabled some of the liquid to be stored after each dilution step, which remained available for further analysis.[13] In an alternative mechanism, oscillatory microfluidics was used to execute stepwise serial dilution *via* coordinated operation of pneumatic valves to first meter both the sample and diluent in separate microfluidic chambers and afterwards mix them through oscillatory liquid manipulation.[14] This process was then repeated to prepare a 6-fold dilution series of a hydrogen peroxide solution and study the oxidative stress in *C. elegans* nematodes. The main drawback of this approach is the need to control each valve individually with an external control unit which makes the device bulky and not compatible with POC applications.

More recently, centrifugal microfluidics has been used to create serial multistep dilutions without the need for multiple external pumps. Here, the liquid manipulation is driven *via* rotational centrifugal forces. Precise control over the disc rotation speed and direction combined with the successful integration of active[15–19] or passive[20–26] valving techniques enabled the execution of fluidic operations such as metering, merging and mixing. A variety of microfluidic designs have been demonstrated to generate both linear[21] and logarithmic[27] dilution series on-chip. Due to the flexibility of the technology, the microfluidic disc design is easily adaptable to meet the dilution and liquid handling requirements of a variety of multistep bioassays.[28–30] The lab-on-a-disc approach, therefore, offers a user-friendly and integrated solution, however, still requires active elements for disc spinning and in some cases valve actuation, limiting their use for POC applications.[31]

To completely overcome the need for any active elements, several capillary-driven microfluidic systems have been developed that enable the sequential delivery of multiple reagents to automate multistep bioassays. For instance, Yafia *et al.* introduced the microfluidic chain reaction concept within a 3D-printed capillary circuit, thereby, automating the sequential reagent delivery accommodating a sandwich enzyme-linked immune detection assay for SARS-CoV-2 antibodies in saliva specimen.[32] Similarly, the research group of Charles Henry established a capillary-driven immunoassay (CaDI) system, which allows the automation of serological assays, among many others, by sequentially delivering reagents to a detection zone.[33,34] In their system, all assay reagents are pre-stored in dried form on the microfluidic device within glass fiber reagent pads which are reconstituted in solution at particular concentrations after sample/buffer application. Despite being extremely promising for automating complex multistep bioassay, these capillary flow-based systems only allow successive delivery of different reagents to a particular detection region. As they always rely on a continuous liquid flow, they do not allow discrete liquid volumes (*i.e.*, liquid slugs) to be diluted and mixed with secondary reagents in a successive manner. More specifically, it is not possible to physically separate the different dilution operations one after the other.

To tackle this, we introduce in this paper another category in which, to our knowledge, for the first time automated and programmable stepwise serial dilution is achieved without the need for any active elements. In particular, a novel passive dilution concept, continuing on the previously developed on-chip metering principle,[35] is presented which allows a discrete sample drop of unknown volume size to be exactly metered and diluted with a dilution factor (DF) between 1 and 10× (and potentially even higher). The module consists of 3 connected microfluidic units in which the structurally encoded fluidic operations of metering, merging and mixing are executed in a stepwise manner by using the coordinated burst action of hydrophobic burst valves (HBVs) (Fig. 1a and b). First, the required number of expansion chambers in the mixing unit (*i.e.*, mixing efficiency) to generate homogeneous solutions is determined for different DFs of 2, 5 and 10×. Next, the dilution accuracy of the microfluidic system is evaluated for each DF by comparing on-chip diluted fluorescent solutions with manually off-chip prepared dilutions. To underpin the modularity and flexibility of the system, three dilution modules are coupled in series to generate $\log_5$ and $\log_{10}$ serial dilutions from which the dilutional linearity (accuracy) is evaluated using fluorescence measurements. Furthermore, the ability of the system to handle low surface tension and crude sample matrices is illustrated to validate its potential for real bioassay sample processing. Finally, fully automated and autonomous serial dilution is achieved by coupling the serially coupled dilution modules to our in-house developed self-powered microfluidic pumping technology (Fig. 1c).[36–39] The results reported in this work demonstrate the advanced sample processing capability of our self-powered microfluidic platform, which now can be further developed towards a variety of (bio)chemical applications.
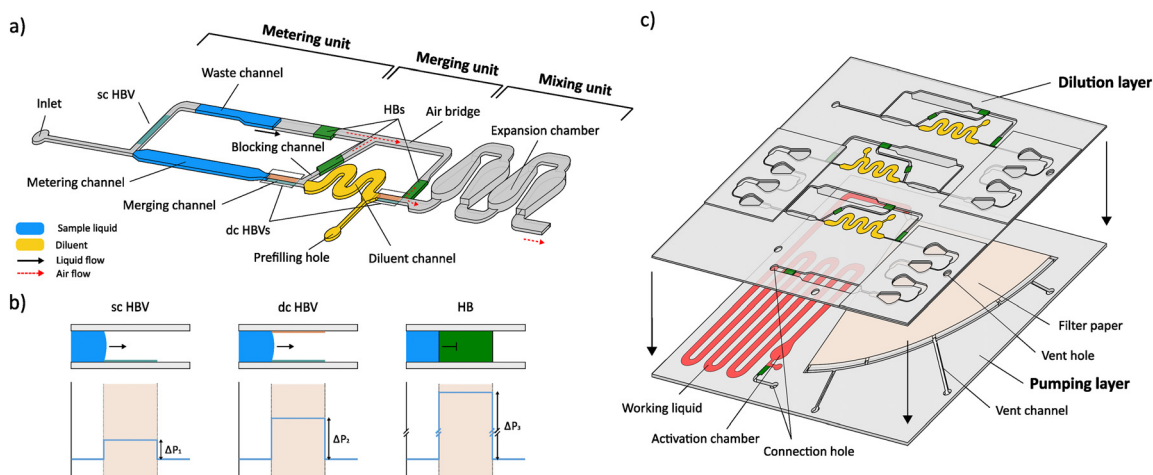
Fig. 1 a) Conceptual design of the dilution module illustrating the 3 microfluidic units that are used for plug metering, merging and mixing, and the positions of the different valving elements (single-coated (sc) and double-coated (dc) HBVs, and hydrophobic barrier (HB)). b) Configuration and working principle of the different valves with their respective theoretical burst pressure profiles. The sc HBV contains a hydrophobic coating at the bottom channel wall while the dc HBV is treated hydrophobic at both the top and bottom walls, resulting in varying burst pressures. The HB comprises a hydrophobic-treated filter paper, which allows air passage but forms a physical barrier for the liquid, hence, inducing a very high burst pressure. c) Conceptual exploded view of the integrated microfluidic device for autonomous multistep serial dilution illustrating the top 'dilution' and bottom 'pumping' layer. The top dilution layer comprises 3 serially coupled dilution modules (5× DF), connected with a connection hole to the bottom pumping layer, holding the prefilled working liquid and wedge-shaped filter paper (Whatman grade 598) of the SIMPLE pump unit.

Materials and methods

Reagents and materials

Polyvinyl chloride (PVC) films of 180 μm thickness were bought at Delbo (Maldegem, Belgium). Double-sided pressure-sensitive adhesive (PSA) tape (200 MP 7956MP) and transfer tape (467MP) with respective thicknesses of 153 and 50 μm were acquired from 3M (Minnesota, USA). Microfluidic dyes were obtained from Darwin Microfluidics (Paris, France). Hydrophobic solutions Aquapel and Fluoropel 800 M were purchased at Aquapel (Pennsylvania, USA) and Cytonix (Maryland, USA), respectively. Whatman quantitative filter paper of grades 43 and 598, fluorescein, bovine serum albumin (BSA) and phosphate buffer saline (PBS) were all obtained from Sigma-Aldrich (Overijse, Belgium). Tween 20 was purchased at Promega (Madison, USA). Left-over EDTA whole blood samples were obtained from the Red Cross Flanders and used within 48 h after receipt.

Microfluidic chip fabrication

Single-step dilution chip. The microfluidic designs for the single-step dilution chips with DFs of 2, 5 and 10× were prepared using Inkscape (Inkscape, USA) vectorial software and fabricated via a rapid layer-by-layer lamination assembly method.[40] In particular, an 80 watt Speedy300 Trotec laser cutter (Trotec Lasers, Austria) was used to pattern the microfluidic circuit in PSA. After channel removal, all hydrophobic barriers (HBs) were manually inserted into their respective positions. These rectangular (1.5 × 3 mm²) pieces of Whatman grade 43 filter paper were cut with a Silhouette blade cutter (Cameo, Silhouette, USA) and treated hydrophobic by overnight impregnation with 1 μL of Aquapel

solution at 50 °C.[35,39] The PSA layer holding the microchannel circuit was finally sealed with PVC films (through manual lamination, see Fig. S6†) that were cut with a KNK Maxx air blade cutter (Klic-N-Kut, USA). Both top and bottom films were locally treated with hydrophobic and superhydrophobic solutions to create single-coated (sc) or double-coated (dc) HBVs after chip closure. Hereto, a mask-based coating strategy was used to locally treat the PVC substrate with Aquapel and Fluoropel and increase the PVC contact angle (~90° untreated) to hydrophobic (~120°) and superhydrophobic (~160°) properties, respectively.[35] Finally, after chip closure, the diluent was prefilled in the diluent channel via a prefilling hole which was sealed afterward.

Autonomous serial dilution chip. The same fabrication method was used to assemble the microfluidic chips for autonomous serial dilution which consisted of two stacked microfluidic layers (see Fig. S6† for the detailed step-by-step assembly protocol). The top layer (dilution layer) holds three microfluidic dilution modules with a DF of 5 or 10×, which were serially connected to achieve a 3-fold logarithmic dilution. In this way total dilutions of 125× and 1000× were obtained, respectively. Underneath, in the pumping layer, a SIMPLE pump unit was integrated as a passive driving source of the liquid manipulation. In particular, a porous material (Whatman grade 598 filter paper) shaped as a circular sector (75°), was inserted in the patterned double PSA layer (306 μm) and its tip was sealed at the top and bottom with a small rectangular strip of transfer tape. Vent holes and channels were foreseen to allow the air present in the porous material of the SIMPLE pump to be expelled out of the chip during working liquid absorption. The latter acted as the fuel of the pump which upon contact with the porous material wicked

in *via* capillary forces and consequently generated a suction force in the connected upstream microfluidic channel network. After chip closure, red-colored (1 : 50 diluted) working liquid and yellow-colored (1 : 20 diluted) diluent were prefilled in the respective working liquid and diluent channels *via* the prefilling holes which were sealed afterward. Both pumping and dilution layers were connected through a connection hole.

Evaluation of mixing efficiency. The mixing efficiency, defined here as the number of required expansion chambers to obtain a homogeneous mixture of the sample and diluent liquid, was determined for dilution modules with varying DFs of 2, 5 and 10×. In particular, dynamic fluorescence measurements of the mixing behaviour were performed by recording the intensity profile of a fluorescein–PBS mixture over the 4 expansion chambers. To do so, a 10 μL droplet of a 1 μg mL^{-1} fluorescein in 1× PBS sample solution was drawn (at 10 μL min^{-1}) through the dilution module utilizing a syringe pump (PHD 2000, Harvard Apparatus, USA). In particular, a syringe pump was connected to the outlet hole of the microfluidic dilution system through microfluidic tubing and used to drive the liquid flow instead of the SIMPLE pump unit. An image of the experimental setup is given in the ESI† (Fig. S7). Depending on the targeted DF (2, 5 or 10×), the metering channel was designed to split off 5, 2 or 1 μL of sample solution and afterwards mix it with 5, 8 or 9 μL of prefilled 1× PBS solution in the downstream diluent channel. A fluorescent microscope (IX71, Olympus Corporation, Japan) and associated HCImageLive software (Hamamatsu Photonic K.K., Japan) were used to record (at 20 frames per second) the fluorescence intensity at 5 specific positions (before the first and after all 4 expansion chambers in the mixing unit). All recorded videos were processed and analyzed using ImageJ (**https://imagej.nih.gov/ij/**, USA) to obtain the intensity profiles at each position. For data visualization, the fluorescence intensity was normalized between 0 and 1, reflecting the minimum and maximum intensity at all measured positions, respectively.

Evaluation of dilution accuracy. The accuracy and reproducibility of the single- and multistep serial dilution systems were evaluated by diluting a fluorescent solution in 1× PBS. For the single-step dilution modules, 12 μL of a 25 μg mL^{-1} fluorescein–PBS stock solution was applied to the chip inlet from which a metered volume (5, 2 or 1 μL) was isolated and subsequently diluted with 5, 8 or 9 μL of prefilled 1× PBS buffer for respective DFs of 2, 5 and 10×. For each DF, at least 4 independent chips were run to assess reproducibility. After the dilution step, 5 μL of the undiluted (liquid fraction that is sent to the storage channel) and the diluted fluorescent solution was transferred out of the chip and post-diluted (manual dilution using pipets) with 20 μL of 1× PBS solution to have sufficient reagent volume to perform the readout. Next, 20 μL of the solution was added to a 384-well plate from which the fluorescence intensity was measured using a spectrophotometer (SpectraMax® iD3, Molecular Devices, USA) at excitation and emission

wavelengths of 480 and 515 nm, respectively. The measured fluorescence intensities were then converted to fluorescein concentrations using a reference calibration curve of manually diluted fluorescein solutions prepared from the same 25 μg mL^{-1} fluorescein stock solution.

The same procedure was executed to determine the performance of the 3-fold logarithmic serial dilution chips. Similar to the mixing efficiency characterization experiments, both the single and multistep dilution systems were run with a syringe pump set at a constant flow rate of 10 μL min^{-1}. Both serial dilutions were plotted as a base-5 or base-10 logarithm of the fluorescence intensity and the accuracy was quantified by linear regression.

Complex sample compatibility. Microfluidic chips, composed of only the mixing unit with four expansion chambers, were assembled to evaluate the compatibility of the system with low surface tension aqueous liquids and crude sample matrices. The presence of bubble formation and the liquid sticking to the channel walls were investigated. Expansion chambers with varying widths (2.0, 1.0, 0.5 and 0.25 mm) of the incoming injection channel were evaluated for both the 1× PBS–1% BSA–0.5% Tween 20 solution (referred to as a wetting liquid hereafter) with low surface tension (~35 mN m^{-1}) and EDTA-stabilized blood samples, mimicking real reagent and sample conditions. Hereto, a syringe pump was used to draw both solutions through the microfluidic chip at a constant flow rate of 10 μL min^{-1}. Additionally, a mixing design incorporating a superhydrophobic treated injection channel (0.25 mm wide) was evaluated using the same setup. This treatment was performed by pipetting 0.5 μL of Fluoropel 800 M solution into the injection channel, followed by a 10 min incubation step at 50 °C before chip closure. Ethical approval (s66604) was obtained from the UZ/KU Leuven ethics committee for all experimental work involving the handling of human blood samples.

Visualization and video processing. The microfluidic behaviour of the coloured liquids within the chips was recorded at 24 fps with a C920 digital webcam (Logitech, Switzerland) mounted in a lightbox (Elviros, USA). The videos were further processed and edited using Hitfilm (Fxhome limited, USA). In-house developed video analysis software (Shapeflow, 10.5281/zenodo.4048741) was used to calculate the applied flow rate of the SIMPLE pump in the autonomous serial dilution chip.

Results and discussion

Working principle

The general working principle of the dilution system is shown in Fig. 2a and Video S1,† which illustrate the different fluidic operations (driven by a syringe pump) that are performed within a dilution module with a 5× DF. First, a precisely metered volume is isolated from the incoming sample liquid by using the coordinated burst action of HBVs with different burst strengths.[35] As is illustrated in
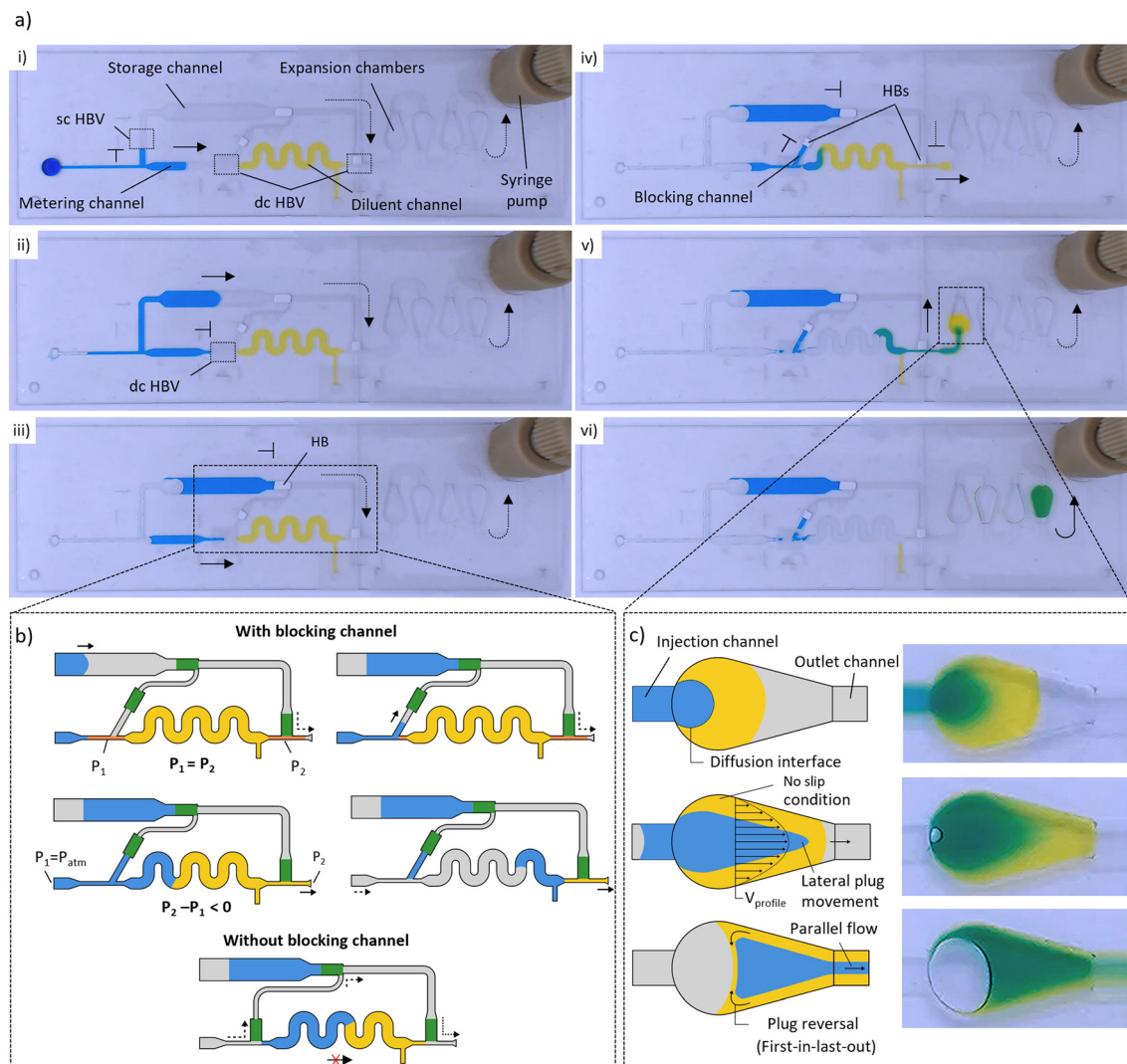
Fig. 2 a) Snapshots of the different liquid manipulations within a dilution module (DF = 5×) illustrating the working principle. (i and ii) The coordinated burst action of HBVs with different burst strengths is used to first isolate a precisely metered sample liquid (2 μL, blue), after which the excess is removed to the storage channel. (iii and iv) The metered sample liquid is next merged with a prefilled diluent (8 μL, yellow) after which (v and vi) the combined plug is sent through a sequence of expansion chambers in which it is mixed into a homogeneous solution. b) Detailed schematics of plug merging, and working principle of the microfluidic air bridge (top). Illustration of failed downstream plug manipulation when no blocking channel is used due to air intake *via* the microfluidic air bridge (bottom). c) Close-up of the expansion chambers, illustrating the three ongoing principles that are used within the mixing process: increase of diffusion interface, parabolic flow profile and lateral plug distribution. Dashed and full arrows indicate air and liquid flow, respectively.

Fig. 2a (i and ii), a sc HBV directs the sample liquid into the metering channel until the liquid front reaches the dc HBV. Due to its higher burst pressure, the dc HBV forces the excess of the sample liquid to burst through the sc HBV and flow into the storage channel after which the liquid in the metering channel becomes isolated. Depending on the desired DF (2, 5 or 10×), the length of the metering channel was adjusted to isolate volumes of 5, 2 or 1 μL (plus the volume of the downstream blocking channel). Evaluating the accuracy of this particular metering step was not part of this paper as it was already studied and confirmed (CV < 3%) in previous work.[32] Downstream, the metering channel is in connection with a diluent channel, here holding 8 μL of diluent liquid (5 or 9 μL for DFs of 2 or 10×, respectively).

The diluent channel is bridged by a microfluidic channel, which diverts the airflow around the diluent liquid and this way prevents it to be manipulated downstream during the first metering step ($P_1 = P_2$) as is explained in Fig. 2b. Only when the sample excess reaches the HB at the end of the storage channel, the metered sample plug is pulled through the dc HBV and merges with the diluent (Fig. 2a (iii) and b). During the bursting of the dc HBV, a small portion of the metered sample volume enters the blocking channel to prevent any airflow to enter the air bridge after plug merging (Fig. 2a (iv) and b). This is an important feature as otherwise only a fraction of the merged plug will be manipulated downstream from the moment the receding liquid front passes the HB (Fig. 2b (bottom)).

The merged sample and diluent plugs are finally manipulated ($P_2 - P_1 < 0$) towards the mixing unit where expansion chambers are used to mix them into a homogeneous solution (Fig. 2a (v and vi)). Like in most passive micromixers, mixing relies mostly on passive diffusion processes, which are generally very slow. To speed up the process, liquids are often flowed side-by-side through microchannels to increase the diffusion interface while simultaneously reducing the diffusion distances.[41] In our system, however, the liquid plugs are positioned one after another that makes the mixing much more complicated as the interface through which diffusion can occur is very limited. The droplet-shaped design of the expansion chambers was selected to be compatible with the layer-by-layer chip assembly process (enabling simple alignment) while enhancing the mixing process through three microfluidic phenomena which are illustrated in Fig. 2c: i) an increased diffusion interface between the plugs due to the 3D expansion in the chamber (height and width, ii) a large flow velocity gradient between the centre (high velocity) and the walls (no-slip condition, low velocity) of the chamber as a result of the parabolic flow profile, and iii) confinement of the merged sample–diluent liquid volume within the expansion chamber to avoid reagent separation. In combination with the parabolic flow profile, a strong lateral plug redistribution is generated which eventually leads to a parallel sample–diluent flow profile in the outgoing channel. Additionally, upon emptying of the expansion chamber, plug reversal is observed as the diluent at the chamber walls is pulled out of the chamber lastly. Therefore, the liquid redistribution within the expansion chamber follows a first-in-last-out flow behaviour. This process is repeated within each chamber until a homogeneous solution is obtained.

Evaluation of mixing efficiency

The mixing of the sample and diluent liquids within the expansion chambers relies mostly on passive diffusion processes as described in the previous section. To determine the number of required chambers to obtain a homogeneous reagent mixture and get more insight into how both liquids are redistributed through them, the fluorescence profile of a fluorescein (1 μg mL^{-1}) plug (diluted in 1× PBS) was recorded over time at 5 different chip positions (Fig. 3a), using an inverted fluorescence microscope (see Video S2† for an example of recording). As shown in Fig. 3b, similar dynamics were observed for dilution modules with DFs of 2, 5 and 10×. At position 1 (Pos-1), the 1× PBS and fluorescein solution can clearly be distinguished over the plug length whereas the large error zones indicate a large fluorescence gradient along the channel width. The fluorescence profile becomes much more stretched and flattened after passing through the first 2 expansion chambers (Pos-2 and Pos-3). This indicates that after 2 chambers, already a significant lateral distribution of the fluorescein solution and diluent has occurred. In chambers 3 and 4 the fluorescence profile is further developed towards a well-defined flat curve with minimal
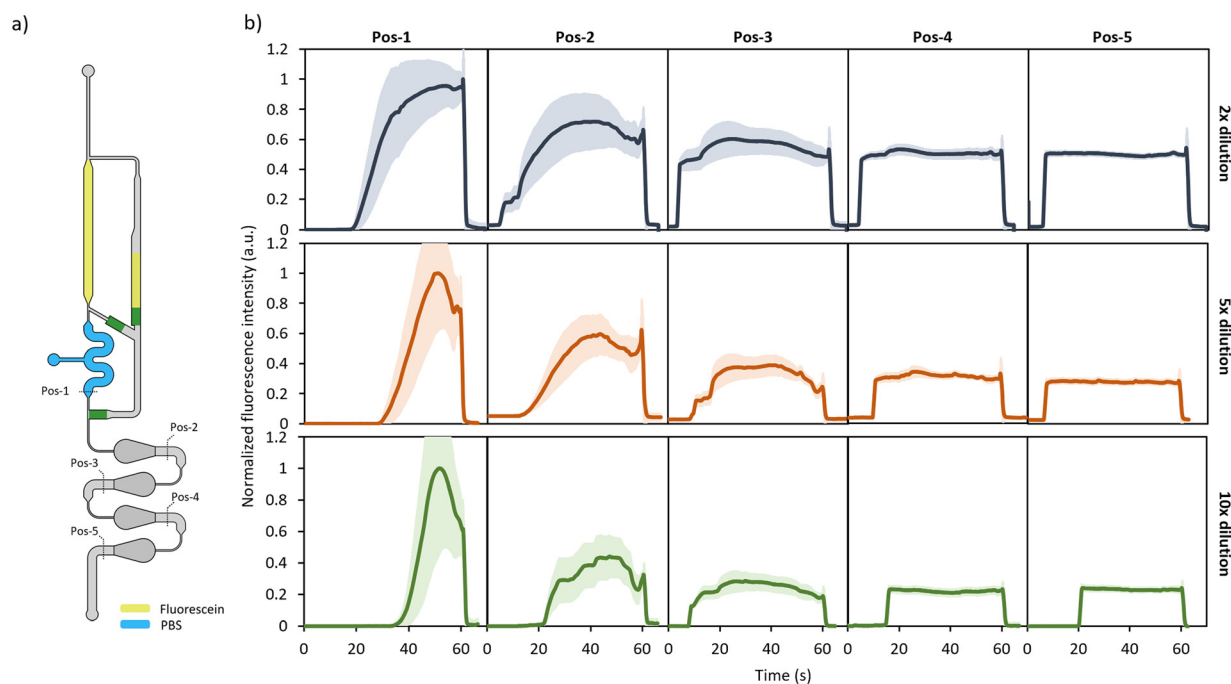

Fig. 3 a) Schematic illustration of the experimental setup for the dilution module (DF = 2×). The dotted lines illustrate the 5 different locations where the fluorescence profile was recorded. b) Evolution of the normalized fluorescence profile of the sample–diluent plug at the different recording positions for dilutions modules with respective DFs of 2, 5 and 10×. The error zones represent the fluorescence intensity distribution (one standard deviation) along the channel width of the measured fluorescence profile.

error zones implying a homogeneous mixture over both the whole length and width of the liquid plug (Pos-4 and Pos-5).

These results show that at least 3 expansion chambers are required to obtain a homogeneous sample–diluent mixture. To always ensure proper mixing, 4 chambers were integrated in the final design of the dilution module. These results are in line with the colorimetric measurements (see Section S1, ESI†) that were performed to evaluate the evolution of the colour distribution within each expansion chamber.

Evaluation of dilution accuracy

Single-step dilution. The accuracy and reproducibility of the dilution module were evaluated by diluting a fluorescein solution in 1× PBS on-chip. The fluorescence intensity of the on-chip diluted and undiluted (liquid fraction that is sent to the storage channel) solution was measured for different DFs of 2, 5 and 10×, and compared with a manually prepared dilution series from the same fluorescein stock solution. The dilution accuracy of the system, calculated here as the ratio between the measured fluorescein concentration of the diluted and undiluted solutions (see Fig. 4 for the measured values), was determined to be in close agreement (no significant difference (paired t-test, $p < 0.05$)) with the intended DF (2.0, 5.2 and 10.7× $vs.$ 2, 5 and 10×). Additionally, the dilution system proved to be reproducible with a CV below 7%. However, a small discrepancy between the undiluted on-chip solution and the undiluted stock dilution was observed. This is illustrated by the blue dotted line in Fig. 4a. The drop in fluorescence signal was confirmed to be a result of non-specific adsorption of the fluorescein molecules to the channel walls (Section S2 ESI†). As a consequence of the hydrophobic properties of the PVC and PSA substrates (respective contact angles of 94° and 120°), proteins, being hydrophobic by nature, tend to stick on the surface. Furthermore, non-specific binding of proteins to the

(super)hydrophobic treated regions of the burst valves might and probably will occur to a certain degree and has to be assessed in more depth once real bioassays are implemented. However, this is not expected to significantly affect the molecule concentration of interest for 2 reasons: (1) the sample liquid will only be in contact with these zones for a very short period (<30 seconds) and (2) the dimensions (area) of the hydrophobic regions which effectively are in contact with the sample solution are very limited. Although the non-specific adsorption does not affect the on-chip dilution accuracy itself (on-chip diluted *versus* undiluted concentration), an absolute lower concentration is obtained relative to the initial concentration of the deposited sample. This can be problematic when exact concentrations have to be achieved. To reduce non-specific adsorption, several methods such as protein (coating with BSA or casein) or chemical (applying hydrophilic coating) blocking of the microchannel have been reported in the literature.[42] To minimize the non-specific protein binding to the HBVs, the size of the hydrophobic treated regions could be drastically reduced (*i.e.*, a single-line coating strategy instead of a patch) resulting in lower surface area to which molecules can stick.

Multi-step serial dilution. The capability of the system to perform 3-fold multistep logarithmic serial dilution was evaluated as well. Hereto, three dilution modules with a DF of either 5× or 10× were coupled in series to obtain a total dilution of 125× and 1000×, respectively. As shown in Fig. 4b, excellent linearity ($R^2 > 0.99$) was obtained for both the $\log_5$ and $\log_{10}$ serial dilutions validating the accurate dilution performance of the system. A discrepancy between the on-chip and the manually prepared dilution series was again observed due to the non-specific binding of the fluorescein to the channel walls. Despite this, the measured fluorescein concentrations (shown next to the datapoints in Fig. 4b) demonstrate consistent and reproducible dilution over the multiple modules. In particular, the regression equations in
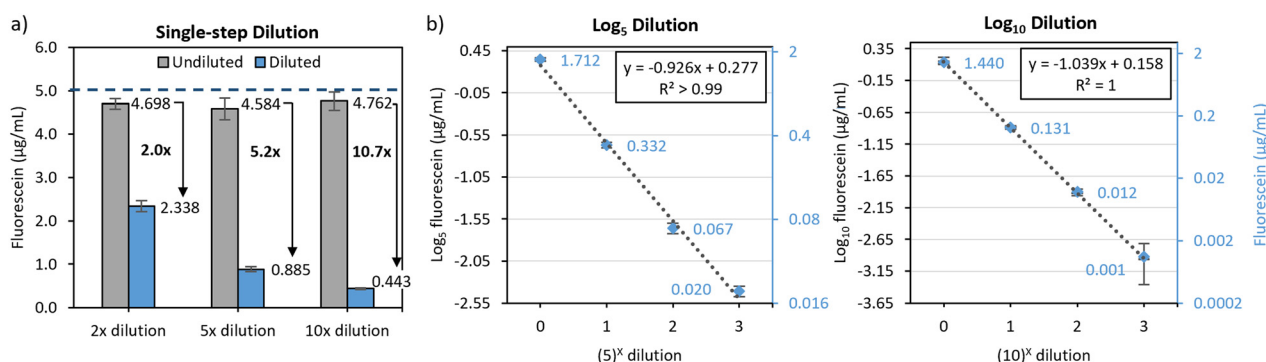

Fig. 4 a) Measured fluorescein concentrations of the undiluted and diluted 5 μg mL⁻¹ fluorescein–PBS solution for single-step dilution modules with DFs of 2, 5 and 10×. The blue dashed line indicates the reference concentration of 5 μg mL⁻¹ while the error bars represent one standard deviation ($n \geq 3$). b) Calibration curves of the on-chip prepared $\log_5$ and $\log_{10}$ dilution series of the stock fluorescein solution (2 μg mL⁻¹) in function of the dilution step (X). Secondary Y-axis (blue) represents logarithmically scaled fluorescein concentrations with base 5 and 10 on the left and right graph, respectively. Grey dotted lines represent the linear fits ($R^2 > 0.99$) to the $\log_5$ or $\log_{10}$ transformed fluorescein concentrations. Values of the measured fluorescein concentrations are added next to the data bars/points. Error bars represent one standard deviation on the measured fluorescein concentration, represented on the secondary Y-axis ($n \geq 3$). All fluorescein intensity values were converted to concentrations by using a fluorescein standard curve which was run in parallel to each experiment ($n = 4$).

Fig. 4b show a slope very close to 1 for both the $\log_5$ and $\log_{10}$ dilution series. This means that for every dilution step (X), $Y = \log_b(C)$ changes by 1 and therefore C changes by a factor b. Here, C represents the fluorescein concentration and b the DF per step, being 5 or 10 in this case. A slope close to 1, hence, confirms that the on-chip dilution accuracy is in good agreement with the targeted DF and remains consistent and reproducible and reproducible over the successive serial dilution steps. The 1000× dilution points show an increased variation, which is not related to the device performance itself but as a consequence of the limited dynamic range of the spectrophotometer. The data prove that the developed dilution module is capable of performing highly accurate multistep serial dilutions with a DF range between 1 and 1000×.

Complex sample matrix compatibility. Because many biological assays use reagents with high protein and surfactant content (*e.g.*, lysis buffer, nucleic acid amplification buffer), the surface tension is reduced and problems with air bubble formation arise when handled in microfluidic systems with abrupt geometrical changes.[43] To evaluate the compatibility of the mixing unit with low surface tension liquids, a wetting solution with high surfactant and protein concentration was run through the expansion chambers while evaluating the liquid behavior. As shown in Fig. 5a, several air bubbles are formed in the

expansion chambers with injection channels wider than 0.25 mm, resulting in a significant amount of liquid loss at the top and bottom of the chamber (Video S3†). For channels with smaller dimensions (0.25 mm) almost no air bubbles are noticed. In a wider channel, the receding liquid–air interface of the liquid plug has a much larger curvature and will therefore pinch sooner at the geometric expansion of the expansion chamber (Fig. 5b). Although a small air fraction can be pulled into the chamber at the pinching interface, the liquid remainders at both sides of the injection channel will creep towards the center of the channel due to the low surface tension. From the moment they reconnect, the airflow becomes interrupted leading to the formation of an air bubble. This process will repeat itself until insufficient liquid remains within the chamber for backflow to occur. By reducing the width of the injection channel, the curvature of the receding liquid–air interface becomes smaller limiting the back flow into the channel.

The system was also evaluated for EDTA-stabilized blood, being an even more challenging matrix due to its non-Newtonian and viscous properties. Again, air bubble formation and liquid loss within the chambers are observed which could not be resolved by channel width reduction (Fig. 5c). To prevent any backflow of the blood into the injection channel, the latter was partly treated superhydrophobic (Fig. 5c right and d bottom). As a consequence, no air bubble formation and liquid loss is present within the chambers as can be seen in Fig. 5c (Video S4†). Additionally, the whole dilution system, including the sample metering and plug merging steps was also validated on whole blood samples as can be seen in Video S5 of the ESI.†

Autonomous platform for serial multistep dilution. An autonomous and integrated microfluidic device that enables serial multistep dilution of a sample liquid without the need for any active pumping elements was finally demonstrated. In this device, a SIMPLE pumping unit[36–39] was integrated into a second 'pumping layer' to drive the liquid manipulation for serial dilution (Fig. 6a). This in-house developed self-powered pumping technology uses the capillary action of a porous paper substrate to absorb a working liquid (red) after activation and generate a suction force in the upstream channel network (Fig. 6b). In particular, by pushing on the activation zone with a fingertip, the pre-filled working liquid is brought in contact with the integrated wedge-shaped filter paper. As a result, the working liquid starts to wick inside the paper substrate due to capillary action. The air inside the pores can escape through vent holes, connecting the porous paper to the outside environment. Upon absorption of the working liquid, a negative pressure gradient is generated upstream the working liquid. This suction force is transferred to the microfluidic circuit of the dilution layer on top through a connection hole connecting the dilution and pumping layers. As a consequence, the sample liquid (blue) is drawn through the
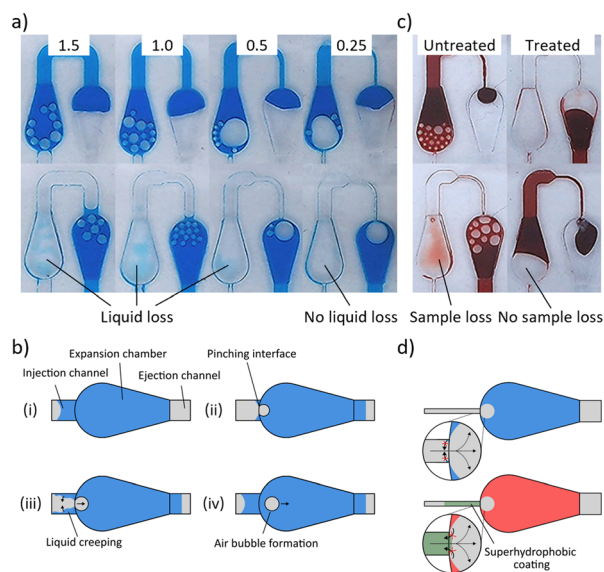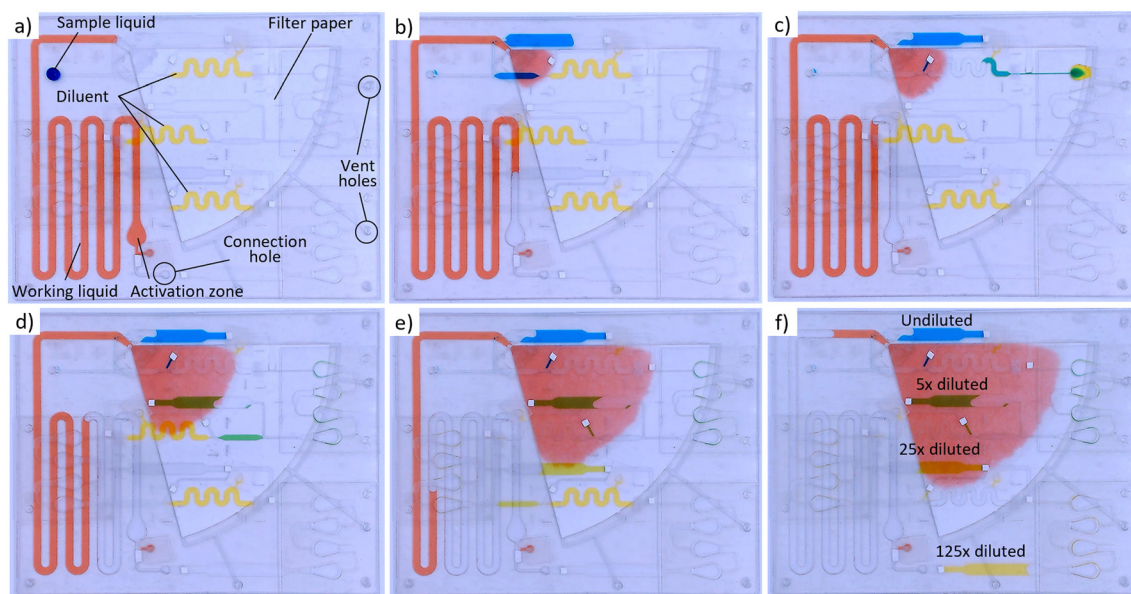

Fig. 5 a) Snapshots of air bubble formation and liquid loss in expansion chambers with injection channels of different widths (1.5, 1.0, 0.5 and 0.25 mm), using PBS–1% BSA–0.5% Tween 20 as a low surface tension sample liquid. b) Schematic illustration of the air bubble formation process within the expansion chambers for low surface tension liquids. c) Snapshots of air bubble formation and liquid loss in expansion chambers with untreated and superhydrophobic treated injection channels (0.25 mm width), using EDTA-stabilized blood as sample liquid. d) Conceptual drawings of implemented strategies to prevent backflow of the sample liquid into the injection channel; (top) channel width reduction and (bottom) superhydrophobic treatment of the injection channel.

Fig. 6 a) Configuration of the autonomous $\log_5$ serial dilution chip with a prefilled diluent and working liquid, and the applied sample liquid drop at the inlet. Snapshots b–f show the different steps of the chip operation where first b) the SIMPLE pump is activated by a finger-press on the activation chamber. After activation, the working liquid is absorbed by the porous paper substrate generating a negative pressure in the dilution layer. As a consequence, the sample liquid is drawn through the different dilution modules (DF = 5×) where consecutive steps of metering and mixing (c–f) are performed. After each dilution step, some of the undiluted, 5×, 25× and 125× diluted solutions are stored in the storage channel.

serially coupled dilution modules (DF of 5× each) of the 'dilution layer' in which it is diluted in a stepwise manner with the prefilled diluents (yellow) as is illustrated in Fig. 6c–f (also see Video S6†). After each dilution step, some of the sample liquid is stored in the storage channel which, if desired, after complete operation can be transferred out of the chip for further use. In this configuration, the 3-fold serial dilution step was completed in <15 min (flow rate of SIMPLE pump ~16 µL min^{-1}), though this can be adjusted, depending on the application, to the desired timing, flow rate and pump capacity by altering the pump angle and dimensions (thickness and radius).[37]

Conclusions

In this paper, we present a novel microfluidic dilution module that can generate multistep serial dilutions in a fully autonomous and programmable way. The mixing efficiency and behaviour of the sample and diluent reagent within the mixing unit were evaluated using dynamic fluorescence measurements, which showed that after 4 expansion chambers a homogeneous reagent mixture was obtained. Comparison of on-chip with manual off-chip dilutions showed good accuracy and reproducibility of the single-step dilution module up to a DF of 10×. Three-fold logarithmic serial dilution ($\log_5$ or $\log_{10}$) was next achieved by coupling 3 dilution modules in series from which the dilution performance was characterized to show excellent linearity ($R^2 > 0.99$) and reproducibility. The compatibility of the system with complex sample matrices was also

validated, clearly illustrating its potential for advanced single- or multi-step sample processing applications. Finally, the self-powered SIMPLE technology was successfully integrated as a passive driving source to manipulate the liquid through the microfluidic network and this way makes the dilution system completely independent of active external equipment.

The ability of the presented microfluidic technology to manipulate discrete sample volumes and consecutively mix them with various liquid reagents in a fully autonomous and programmable way is unprecedented in the field of passive microfluidics. Moreover, its modularity and plug-and-play principle allow the configuration of the microfluidic circuit to be programmed (in terms of the number of dilution steps and DFs) towards tailored applications with great ease. We, therefore, strongly believe that the advances presented in this work contribute significantly to the development of next-generation lab-on-a-chip devices with integrated complex multistep sample processing capability. The latter being a critical aspect hampering the widespread adoption and implementation of POC diagnostic tests in real world settings. The performance of nucleic acid amplification assays, for example, is mostly still restricted to laboratory environments as a consequence of their complex sample processing requirements (i.e., sample lysis, post-dilution, mixing with amplification reagents, etc.). In our opinion, these steps can all be integrated and automated on the presented platform, which will be the objective of our future research.

Author contributions

Conflicts of interest

The authors declare the following competing financial interest(s): D. V., F. D. D., and J. L. are inventors of a pending patent application for the microfluidic dilution device. The remaining authors have no conflicts of interest to declare.

Acknowledgements

Notes and references

1 J. Park, D. H. Han and J. K. Park, *Lab Chip*, 2020, **20**, 1191–1203.
2 M. Urdea, L. A. Penny, S. S. Olmsted, M. Y. Giovanni, P. Kaspar, A. Shepherd, P. Wilson, C. A. Dahl, S. Buchsbaum, G. Moeller and D. C. Hay Burgess, *Nature*, 2006, **444**, 73–79.
3 N. L. Jeon, S. K. W. Dertinger, D. T. Chiu, I. S. Choi, A. D. Stroock and G. M. Whitesides, *Langmuir*, 2000, **16**, 8311–8316.
4 S. K. W. Dertinger, D. T. Chiu, N. L. Jeon and G. M. Whitesides, *Anal. Chem.*, 2001, **73**, 1240–1246.
5 C. W. Chang, Y. J. Cheng, M. Tu, Y. H. Chen, C. C. Peng, W. H. Liao and Y. C. Tung, *Lab Chip*, 2014, **14**, 3762–3772.
6 E. Jastrzebska, S. Flis, A. Rakowska, M. Chudy, Z. Jastrzebski, A. Dybko and Z. Brzozka, *Microchim. Acta*, 2013, **180**, 895–901.
7 M. Hosokawa, T. Hayashi, T. Mori, T. Yoshino, S. Nakasono and T. Matsunaga, *Anal. Chem.*, 2011, **83**, 3648–3654.
8 F. Lin, W. Saadi, S. W. Rhee, S. J. Wang, S. Mittal and N. L. Jeon, *Lab Chip*, 2004, **4**, 164–167.
9 C. Kim, K. Lee, J. H. Kim, K. S. Shin, K. J. Lee, T. S. Kim and J. Y. Kang, *Lab Chip*, 2008, **8**, 473–479.
10 K. Lee, C. Kim, B. Ahn, R. Panchapakesan, A. R. Full, L. Nordee, J. Y. Kang and K. W. Oh, *Lab Chip*, 2009, **9**, 709–717.
11 N. Vasilakis, K. I. Papadimitriou, H. Morgan and T. Prodromakis, *Sensors*, 2019, **19**, 911.
12 B. M. Paegel, W. H. Grover, A. M. Skelley, R. A. Mathies and G. F. Joyce, *Anal. Chem.*, 2006, **78**, 7522–7527.
13 S. Ahrar, M. Hwang, P. N. Duncan and E. E. Hui, *Analyst*, 2014, **139**, 187–190.
14 C. Wang, S. Zhao, X. Zhao, L. Chen, Z. Tian, X. Chen and S. Qin, *Biomicrofluidics*, 2019, **13**, 024105.
15 T. H. Kim, C. J. Kim, Y. Kim and Y. K. Cho, *Sens. Actuators, B*, 2018, **256**, 310–317.
16 K. Abi-Samra, R. Hanson, M. Madou and R. A. Gorkin, *Lab Chip*, 2011, **11**, 723–726.
17 J. M. Park, Y. K. Cho, B. S. Lee, J. G. Lee and C. Ko, *Lab Chip*, 2007, **7**, 557–564.
18 T. Kawai, N. Naruishi, H. Nagai, Y. Tanaka, Y. Hagihara and Y. Yoshida, *17th Int. Conf. Miniaturized Syst. Chem. Life Sci. MicroTAS*, 2013, vol. 2, pp. 961–963.
19 H. Hwang, Y. Kim, J. Cho, J. Lee, M. S. Choi and Y. K. Cho, *Anal. Chem.*, 2013, **85**, 2954–2960.
20 D. J. Kinahan, S. M. Kearney, O. P. Faneuil, M. T. Glynn, N. Dimov and J. Ducrée, *RSC Adv.*, 2015, **5**, 1818–1826.
21 M. Tang, X Huang, Q. Chu, X. Ning, Y. Wang, S. Kong, X. Zhang, G. Wang and H. Ho, *Lab Chip*, 2018, **18**, 1452–1460.
22 T. H. G. Thio, S. Soroori, F. Ibrahim, W. Al-Faqheri, N. Soin, L. Kulinsky and M. Madou, *Med. Biol. Eng. Comput.*, 2013, **51**, 525–535.
23 M. Bauer, M. Ataei, M. Caicedo, K. Jackson, M. Madou and L. Bousse, *Microfluid. Nanofluid.*, 2019, **23**, 1–12.
24 R. Gorkin, C. E. Nwankire, J. Gaughran, X. Zhang, G. G. Donohoe, M. Rook, R. O'Kennedy and J. Ducrée, *Lab Chip*, 2012, **12**, 2894–2902.
25 H. Hwang, H. H. Kim and Y. K. Cho, *Lab Chip*, 2011, **11**, 1434–1436.
26 D. J. Kinahan, S. M. Kearney, N. Dimov, M. T. Glynn and J. Ducrée, *Lab Chip*, 2014, **14**, 2249–2258.
27 P. Juelg, M. Specht, E. Kiphf, M. Lehnert, C. Eckert, T. Hutzenlaub, F. von Stetten, R. Zengerle and N. Paust, *Lab Chip*, 2019, **19**, 2205–2219.
28 B. S. Lee, Y. U. Lee, T. h. Kim, J. Park, J. G. Lee, J. Kim, H. Kim, W. G. Lee and Y. K. Cho, *Lab Chip*, 2011, **11**, 70–78.
29 T. Abe, S. Okamoto, A. Taniguchi, M. Fukui, A. Yamaguchi, Y. Utsumi and Y. Ukita, *Anal. Methods*, 2020, **12**, 4858–4866.
30 B. D. Henderson, D. J. Kinahan, J. Rio, R. Mishra, D. King, S. M. Torres-Delgado, D. Mager, J. G. Korvink and J. Ducrée, *Biosensors*, 2021, **11**, 73.
31 I. J. Michael, T. H. Kim, V. Sunkara and Y. K. Cho, *Micromachines*, 2016, **7**, 32.
32 M. Yafia, O. Ymbern, A. O. Olanrewaju, A. Parandakh, A. S. Kashani, J. Renault, Z. Jin, G. Kim, A. Ng and D. Juncker, *Nature*, 2022, **605**, 644–649.

33 C. Carrell, I. Jang, J. Link, J. S. Terry, Z. Call, Y. Panraksa, O. Chailapakul, D. S. Dandy, B. J. Geiss and C. S. Henry, *Anal. Methods*, 2023, **15**, 2721.

34 J. S. Link, C. S. Carell, I. Jang, E. J. O. Barstis, Z. D. Call, R. A. Bellows, J. J. O'Donnell-Sloan, J. S. Terry, L. B. R. Anderson, Y. Panraksa, B. J. Geiss, D. S. Dandy and C. S. Henry, *Anal. Chim. Acta*, 2023, **1277**, 311634.

35 D. Vloemans, L. Van Hileghem, W. Verbist, D. Thomas, F. Dal Dosso and J. Lammertyn, *Lab Chip*, 2021, **21**, 4445–4454.

36 F. Dal Dosso, T. Kokalj, D. Spasic and J. Lammertyn, in *Proceedings of the 20th International Conference on Miniaturized systems for Chemistry and Life Sciences. µTAS*, 2016, pp. 990–991.

37 F. Dal Dosso, Y. Bondarenko, T. Kokalj and J. Lammertyn, *Sens. Actuators, A*, 2019, **287**, 131–137.

38 F. Dal Dosso, T. Kokalj, J. Belotserkovsky, D. Spasic and J. Lammertyn, *Biomed. Microdevices*, 2018, **20**, 44.

39 F. Dal Dosso, L. Tripodi, D. Spasic, T. Kokalj and J. Lammertyn, *ACS Sens.*, 2019, **4**, 694–703.

40 P. K. Yuen and V. N. Goral, *Lab Chip*, 2010, **10**, 384–387.

41 K. Ward and Z. H. Fan, *J. Micromech. Microeng.*, 2015, **25**, 094001.

42 J. Y. Lichtenberg, Y. Ling and S. Kim, *Sensors*, 2019, **19**, 2488.

43 A. O. Olanrewaju, A. Robillard, M. Dagher and D. Juncker, *Lab Chip*, 2016, **16**, 3804–3814.